Novel STY/nBA/GMA and STY/nBA/MAA Core−Shell Latex Blends: Film Formation, Particle Morphology, and Cross-Linking. 20. A Spectroscopic Study†

Yaqiu Zhao and Marek W. Urban*

The University of Southern Mississippi, School of Polymer and High Performance Materials, Shelby F. Thames Polymer Research Center, Hattiesburg, Mississippi 39406

Received April 10, 2000; Revised Manuscript Received August 18, 2000

ABSTRACT: These studies focus on behavior of sodium dioctylsulfosuccinate (SDOSS) surfactant molecules in styrene/*n*-butyl acrylate/glycidyl methacrylate (Sty/nBA/GMA) and styrene/*n*-butyl acrylate/methacrylic acid (Sty/nBA/MAA) blended latexes during their film formation process. Using a combination of Fourier transform infrared (FT-IR) microanalysis and FT-Raman techniques, not only stratification of SDOSS surfactant molecules during film formation process can be assessed but also the effect of latex particle structures and cross-linking reactions during coalescence can be determined. For Sty/nBA/GMA and Sty/nBA/MAA blended copolymer latexes, SDOSS exhibit nonuniform distributions at the film air (F−A) interface. However, for core/shell Sty/nBA-GMA and Sty/nBA-MAA blended latexes, SDOSS is distributed uniformly near the F−A interface, and its concentration levels are lower as compared to copolymer latex blends. At elevated coalescence temperatures, SDOSS migration to the F−A interface is prohibited due to cross-linking reactions between epoxy and acid groups. Microanalysis results show that SDOSS migration to the F−A interface is initiated after the majority of H_2O (>95%) evaporates from the film. Furthermore, these studies show that latex particle surface morphology, particle−particle interdiffusion, and cross-linking reactions play a significant role in controlling mobility of low molecular weight species in latex films.

Introduction

Acrylate emulsion polymers containing epoxies or acid functional groups are widely used in many applications[1,2] because these reactive groups facilitate cross-linking reactions, thus enhancing physical and chemical integrity of coalesced latex films. As a result, impact strength, tensile, cohesion strength, and chemical resistance may be altered.[3,4] In essence, utilization of physical coalescence and chemical reactivity represent a combination of thermoplastic and thermosetting processes which involve water evaporation, latex particle packing, particle deformation, and coalescence with interparticle diffusion of polymer chains and cross-linking reactions.[5] If the kinetics of cross-linking reactions within individual latex particles exceeds particle interdiffusion across particle−particle boundaries, latex films may exhibit limited coalescence. However, if these processes are conducted at appropriate rates, desirable film formation and controllable properties will be achieved.

Previous studies on thermoplastic latex films indicated that mobility of low molecular weight anionic surfactants may be affected by latex glass transition temperature (T_g), and subsequently, free volume of a polymer matrix,[6,7] surface tension at the film−air (F−A) and film−substrate (F−S) interfaces,[8−13] compatibility,[14−22] coalescence times,[14−24] and latex particle structures.[25,26] In view of the above considerations, surfactant behavior in thermosetting type latex film formation processes has not been addressed. Therefore, in an effort to further advance our understanding of the effect of cross-linking reactions on film formation, this study focuses on synthesis and molecular level assessments of blended latexes containing controllable and precisely defined quantities of styrene (Sty), *n*-butyl acrylate (nBA), glycidyl methacrylate (GMA), methacrylate acid (MAA) moieties. Four types of latexes are synthesized: random copolymer p-(Sty/nBA/GMA) and p-(Sty/nBA/MAA) and core/shell p-(Sty/nBA-GMA) and p-(Sty/nBA-MAA) were copolymerized in such a way that the majority of epoxy or acid groups are present on latex particle surfaces by adding functional monomers during the final stages of synthesis. In this contest, sodium dioctylsulfosuccinate (SDOSS) migration in blended random copolymer p-(Sty/nBA/GMA) and p-(Sty/nBA/MAA) (1:1 w/w % ratio) (blend A) and core/shell p-(Sty/nBA-GMA) and p-(Sty/nBA-MAA) (1:1 w/w % ratio) (blend B) latex films will be examined and compared to blend C, which is a 1:1 mixture of p-Sty and p-nBA latexes. An ultimate goal of such an experimental design comes from the fact that latex particle structures and competing processes between particle interdiffusion and cross-linking reactions during coalescence may affect numerous film properties, including surfactant distribution across latex films.

Experimental Section

Reagents. Styrene (Sty), *n*-butyl acrylate (nBA), glycidyl methacrylate (GMA), methacrylic acid (MAA), sodium dioctylsulfosuccinate (SDOSS), potassium persulfate ($K_2S_2O_8$), *tert*-butyl hydroperoxide (*t*-BHP), and sodium bicarbonate ($NaHCO_3$) were purchased from Aldrich Chemical Co. Vanadium(IV) oxide sulfate and ascorbic acid were purchased from Merck, Inc.

Latex Preparation. Preparation of Polystyrene Seeds. The p-Sty seed latexes were prepared batch wise in a 500 mL glass reactor by emulsion polymerization at 75 °C using $K_2S_2O_8$ as an initiator and SDOSS as the surfactant (Table 1). The reactor was charged with a mixture containing Sty, DDI, SDOSS, and $NaHCO_3$ purged with N_2, and heated to 75 °C.

* To whom all correspondence should be addressed.

† Parts 1−19 were published in *Macromolecules* and *J. Appl. Polym. Sci.* (1991−2000).

10.1021/ma000625h CCC: $19.00
Published on Web 10/13/2000

Table 1. p-Sty Seeds, Core/Shell p-(Sty/nBA-GMA), p-(Sty/nBA-MAA), and Randomly Copolymerized p-(Sty/nBA/GMA) and p-(Sty/nBA/MAA) Latex Parameters and Starting Components:

latex	p-Sty seeds	core/shell p-(Sty/nBA-GMA)	core/shell p-(Sty/nBA-MAA)	p-(Sty/nBA/GMA)	p-(Sty/nBA/MAA)
particle size (nm)	61 ± 5	89 ± 10	86 ± 10	102 ± 10	86 ± 10
components					
DDI (%)	80.8	53.0	53.6	62.8	63.9
p-Sty seed (19.1% solids) (%)		37.9	38.3		
styrene (%)	18.3			16.06	16.36
n-butyl acrylate (%)		6.92	7.0	16.06	16.36
glycidyl methacrylate (%)		1.20		2.79	
tert-butyl hydroperoxide (%)		0.22		0.285	
ascorbic acid (%)		0.45		0.58	
vanadium oxide sulfate (%)		0.004		0.0048	
SDOSS (%)	0.73	0.30	0.31	1.35	1.38
methacrylic acid (%)			0.74		1.72
$NaHCO_3$ (%)	0.06				
$K_2S_2O_8$ (%)	0.11		0.061	0.063	0.207

At that point, 30 mL of $K_2S_2O_8$ solution (0.014 g/mL) was added. Polymerization was allowed to proceed for 3 h, and this process was monitored using FT-Raman spectroscopy by measuring the intensity of the 1634 cm^{-1} band attributed to the C═C vibrations of styrene. The process was discontinued until the 1634 cm^{-1} band was nondetectable. p-Sty seed latex particle size (61 ± 5 nm) was measured using transmission electron microscopy (TEM) (JEM-100S, JEOL), and the micrographs are illustrated in Figure 1a.

Effect of Initiator on Synthesis of Latex Shell Containing Epoxies. Since epoxy functionalities are to be incorporated onto p-Sty seeds, the first step in this process is to realize that epoxy functionalities may react with H_2O at elevated temperatures. Thus, it is necessary to optimize synthesis conditions in such a way that these groups remain active on the surface of latex particles. For that reason, redox (*t*-BHP, vanadium(IV) oxide sulfate, and ascorbic acid) and thermolysis ($K_2S_2O_8$) initiators were compared in the synthesis of core/shell GMA latexes, and the reactions were conducted at 25 and 75 °C, respectively. FT-Raman spectroscopy was used to monitor epoxy functionalities, and the results are illustrated in Figure 2. Traces A, B, C, and D of Figure 2 illustrate FT-Raman spectra of GMA, p-(Sty/nBA/GMA) copolymer, core/shell p-(Sty/nBA-GMA) synthesized at 25 °C, and core/shell p-(Sty/nBA-GMA) synthesized at 75 °C, respectively. Comparison of these spectra clearly indicates that the 1260 cm^{-1} band due to epoxy ring breathing modes[27] is detectable for the GMA copolymer when the redox initiator was used at 25 °C (traces B and C). However, the epoxy at 1260 cm^{-1} disappears when thermolysis initiator is used at 75 °C (trace D), indicating that, in an effort to maintain epoxy functionalities, GMA copolymer synthesis should be conducted under redox conditions.

Core/Shell Latex Particles. Core/shell Sty/nBA-MAA latex was synthesized using a semibatch polymerization process. DDI and p-Sty seeds were first charged into the reactor and heated to 75 °C, with a continuous N_2 purge. A 20 mL aliquot of $K_2S_2O_8$ solution (0.008 g/mL) and 130 mL of pre-emulsion of nBA + DDI + SDOSS + MAA were charged using separated valves. FT-Raman spectroscopy was used to monitor the C═C band intensity at 1634 cm^{-1} until all the monomers were consumed. The overall reaction time was about 4 h. A chemical makeup of starting materials for Sty/nBA-MAA core/shell polymer latex is summarized in Table 1.

A core/shell Sty/nBA-GMA latex was synthesized using the redox initiator system, and reaction was conducted at 25 °C. DDI, p-Sty seed, ascorbic acid, and vanadium oxide sulfate were first charged into the reactor while continuously purged with N_2. Ascorbic acid and vanadium(IV) oxide sulfate were components of the redox initiator system. A 20 mL aliquot of *t*-BHP initiator solution (0.0295 g/mL) and 142 mL of pre-emulsion of *n*-BA + DDI + SDOSS + GMA were charged using separate valves at the same time. Initiator and pre-emulsion feeding rate were 10 and 20 mL/h, respectively, and their additions were completed at the same time. Again, FT-Raman spectroscopy was used to monitor the C═C band intensity at 1634 cm^{-1} until all monomers were consumed. This process

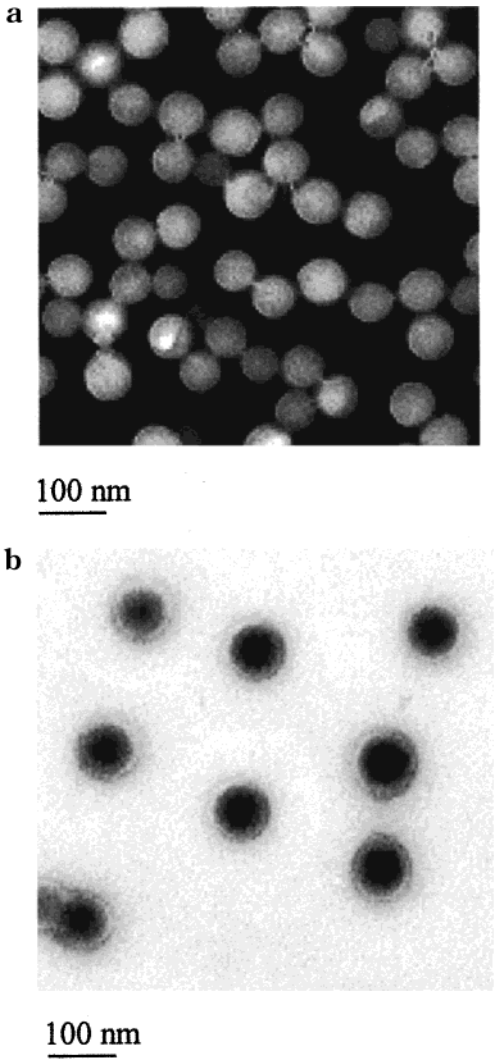

Figure 1. TEM micrographs of latex particles. (a) p-Sty seeds: an average particle size of 61 ± 5 nm. (b) Sty/nBA-GMA core/shell particles: an average particle size of 89 ± 10 nm.

provides relatively uniform shell of nBA-GMA copolymer surrounding the p-Sty core. The results of TEM (JEM-100S, JEOL) analysis are illustrated in Figure 1b, showing an average particle size of 89 ± 10 nm. As illustrated in Figure 1b, the core/shell latex was stained with phosphotungestic acid (PTA) to protect the polymer particles from deforming under an electron beam, and ruthenium tetroxide (RuO_4) was used to stain the p-Sty-rich regions.[28] It is quite apparent that the core−shell morphology was obtained and a p-Sty core appears

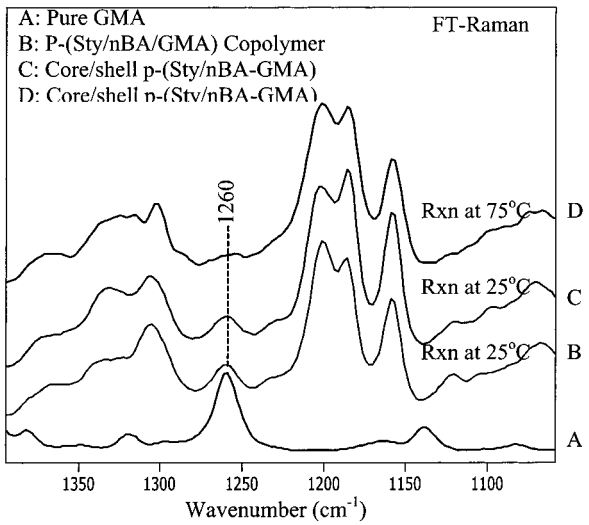

Figure 2. FT-Raman spectra in the 1400−1050 cm^{-1} region of latexes: (A) pure GMA; (B) p-(Sty/nBA/GMA) copolymer latex (reaction temperature: 25 °C); (C) p-(Sty/nBA-GMA) core/shell latex (reaction temperature: 25 °C); (D) p-(Sty/nBA-GMA) core/shell latex (reaction temperature: 75 °C).

as dark phase, whereas p-(nBA-GMA) shell exhibits lighter circular appearance.

Copolymer Latexes. As described elsewhere,[17,18] Sty/nBA/MAA copolymer latex was synthesized by a semicontinuous emulsion polymerization. Sty/nBA/GMA latex was synthesized using redox initiator system at 25 °C because GMA epoxy groups are able to hydrolyze at 75 °C if $K_2S_2O_8$ is used as an initiator. A 50 mL aliquot of DDI and 1.0 g of SDOSS were charged into a 500 mL glass reactor under continuous N_2 purge at 75 °C. A 24 mL aliquot of pre-emulsion 1 (42.1 w/w % DDI, 28.2 w/w% Sty, 28.2 w/w% nBA, and 1.1 w/w% SDOSS) was charged into reactor, followed by addition of 7 mL of $K_2S_2O_8$ initiator solution (0.0186 g/mL). After 30 min, the reactor is cooled to 25 °C; ascorbic acid and vanadium oxide sulfate were charged into the reactor. A 100 mL aliquot of pre-emulsion 2 (39.9 w/w% DDI, 26.5 w/w% nBA, 26.5 w/w% Sty, 5.76 w/w% GMA, and 1.34 w/w% SDOSS) and 23 mL of *t*-BHP initiator solution (0.026 g/mL) were charged into reactor at the same time using separated valves. During the second stage, initiator and pre-emulsion 2 feeding rate were 6.0 and 33.3 mL/h, respectively, and their additions were completed at the same time. FT-Raman was used to monitor the C=C band at 1634 cm^{-1} until all the monomers were consumed. A chemical makeup of the starting materials for Sty/nBA/MAA copolymer latex is summarized in Table 1.

Film Preparation. Prior to the preparation of latex films, all latex dispersions were diluted to 15% w/w solids using DDI. Figure 3 provides definitions of latex blends synthesized and examined in this study. Blend A was obtained by mixing random copolymer p-(Sty/nBA/GMA) and p-(Sty/nBA/MAA) in 1:1 w/w % ratio, stirred, and allowed to store for 10 days before coalescence. Blend B was prepared in the same way, but core/shell copolymer p-(Sty/nBA-GMA) and p-(Sty/nBA-MAA) were used. Such latex blends were cast on poly(tetrafluoroethylene) (PTFE) substrate and allowed to coalescence at 80% relative humidity (RH) for 3 days at 25 °C or coalesced at high temperature for 2 h in an oven, followed by cooling it down to 25 °C. In a typical experiment, approximately 100 μm thick dry films were prepared.

Spectroscopic Measurements and Latex Film Analysis. ATR FT-IR spectra were collected on a Nicolet Magna-850 FT-IR single beam spectrometer at 4 cm^{-1} resolution and a mirror speed of 0.1581 cms^{-1}. A KRS-5 crystal with a 45° angle 50 × 20 × 3 mm was used. Each spectrum represents 200 co-added scans ratioed to 200 scans collected on an empty ATR cell. All spectra were corrected for spectral distortions and optical effects using Q-ATR software.[29] Microscopic ATR FT-IR spectra were collected using IRμs/Nic-Plan molecular microanalysis system (Nicolet Instruments, Inc.). Latex samples were analyzed using ATR objective in a reflectance mode and equipped with a ZnSe crystal. Surfaces were mapped using a constant contact pressure between the ZnSe crystal and latex specimens. Each spectrum was recorded at 4 cm^{-1} resolution, and 200 scans were co-added using a 3.2 mm circular aperture. In a typical experiment, an ATR probe analyzes approximately 50−100 μm surface area, and the source of an ATR signal comes from about 3 μm below the surface.[29]

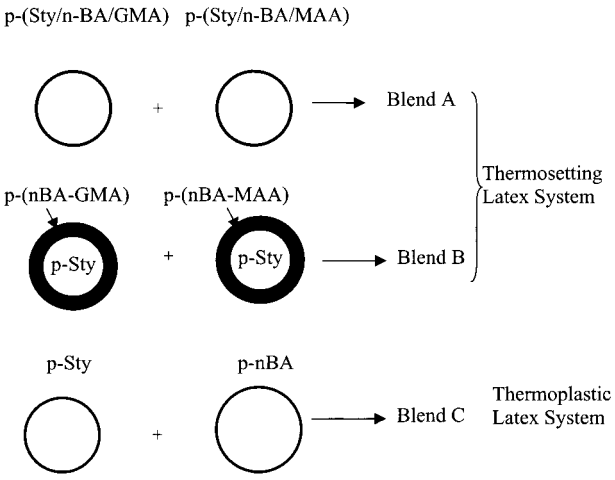

Figure 3. Schematic diagram of latex blends: blend A, 1.0:1.0 w/w % of p-(Sty/nBA/GMA) and p-(Sty/nBA/MAA) copolymer latexes; blend B, 1.0:1.0 w/w % of p-(Sty/nBA-GMA) and p-(Sty/nBA-MAA) core/shell latexes; blend C, 1.0:1.0 w/w % of p-Sty (102 nm) and p-nBA (150 nm) homogeneous latexes.

FT-Raman spectra were measured using an IFS 55/FRA 106 FT-IR/Raman spectrometer (Bruker Instruments, Inc.). As an excitation source, a diode pumped Nd:YAG laser was used to provide a maximum power of 500 mW at the sampling area. Opus software (Bruker Instruments, Inc.) was used to analyze spectra.

Glass transition temperatures (T_g) of latex films were measured using a dynamic mechanical thermal analysis instrument (Rheometric Scientific, DMTA 3E). Dry latex films were cut into 10 × 30 mm. The thickness of each specimen was approximately 100 μm. The DMTA scans were performed using a dynamic temperature ramp of 3 °C/min, a fixed oscillating frequency of 1 Hz, and a controlled strain of 0.5% in the temperature range from −100 to 200 °C. For blend A, a single T_g detected using DMTA is 15 °C. As expected, two T_g's are detected for blend B at 10 and 120 °C, which are due to its core/shell polymers. For blend C, also two T_g's at −35 and 110 °C are detected, which are due to p-nBA phase and p-Sty phase.

The degree of cross-linking was evaluated on the basis of swelling experiments[30] using latex films, which coalesced at 25 °C for 3 days, followed by annealing latex films at 50, 75, 90, 120, 160, and 180 °C for 2 h. Latex films (0.1−0.2 g) were immersed in acetone for 48 h at room temperature. Samples were reweighed after drying at 50 °C for 24 h, and the gel content was determined using the following equation:

$$\text{gel content (\%)} = \frac{\text{weight of dry gel} \times 100}{\text{weight of initial latex film}}$$

Results and Discussion

Although the primary objective of these studies is to elucidate the effect of latex particle structures and competing cross-linking/diffusion processes on surfactant behavior, an ultimate goal is to synthesize functionalized latexes and understand their coalescence. As described in the Experimental Section, micrographs illustrated in Figure 1 clearly illustrate that indeed synthesized latex particles exhibit core/shell structures,

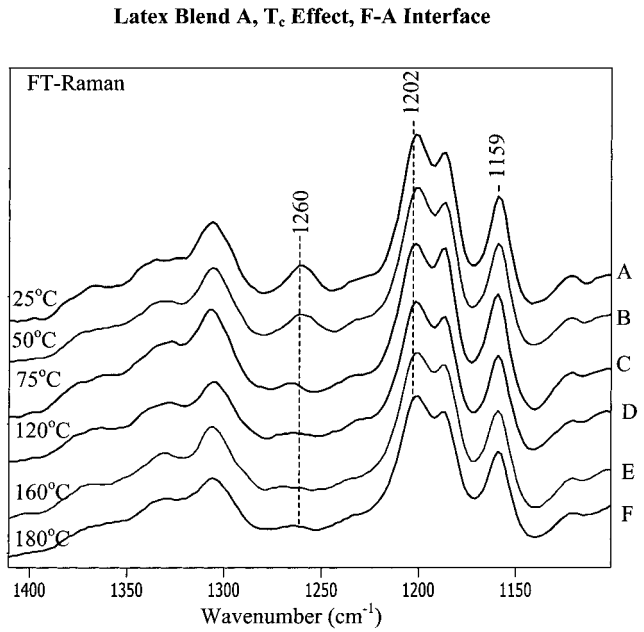

Figure 4. FT-Raman spectra in the 1420−1100 cm^{-1} region of blend A films coalesced at different temperatures: (A) 25 °C; (B) 50 °C; (C) 75 °C; (D) 120 °C; (E) 160 °C; (F) 180 °C.

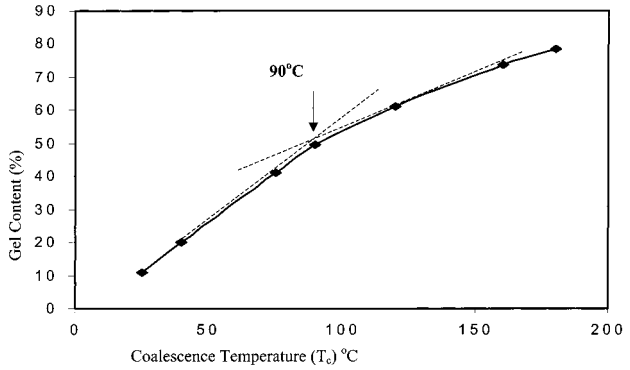

Figure 5. Gel content (%) plotted as a function coalescence temperature for blend A.

with *p*-Sty seeds shown in Figure 1a and *p*-(Sty/*n*-BA-GMA) core/shell particles in Figure 1b. As shown in Figure 3, we will focus on three latex blends: blend A, a 50/50% mixture of thermosets of randomly copolymerized *p*-(Sty/*n*-BA/GMA) and *p*-(Sty/*n*-BA/MAA); blend B, a 50/50% mixture of core/shell type *p*-(Sty/*n*-BA-GMA) and *p*-(Sty/*n*-BA-MAA); blend C, a 50/50% mixture of *p*-Sty and *p*-*n*-BA. The Results and Discussion section is divided into several sections discussion specific phenomena and their relationship to surfactant stratification.

Cross-Linking Reactions and Glass Transition Temperature. As first step, let us determine the extent of cross-linking during coalescence of blends A and B. The extent of cross-linking reactions between epoxy and COOH groups was examined by monitoring consumption of epoxy functionalities using FT-Raman spectroscopy and by measuring the gel content. Figure 4 illustrates FT-Raman spectra of blend A coalesced at temperatures ranging from 25 to 180 °C (traces A−F). As seen, a decrease of the 1260 cm^{-1} band due to epoxy functionalities is detected when coalescence temperature (T_c) increases. As expected, the 1260 cm^{-1} band is practically nondetectable when $T_c = 120$ °C, indicating that all epoxies reacted with acid groups during coalescence. At this point it is appropriate to conduct parallel experiments that would allow us to evaluate the amount of cross-linking in blends A and B coalesced at different temperatures. This can be accomplished by conducting swelling experiments,[30] and Figure 5 illustrates a plot of the gel content as a function of temperature.

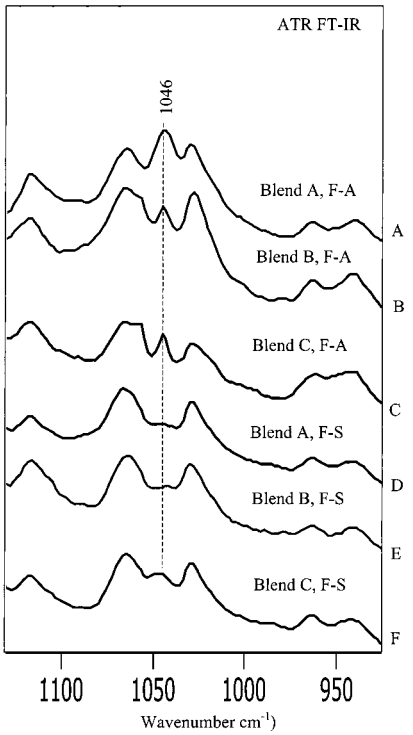

Figure 6. ATR FT-IR spectra in the 1130−920 cm^{-1} region of blended latexes: (A) blend A (F−A interface); (B) blend B (F−A interface); (C) blend C (F−A interface); (D) blend A (F−S interface); (E) blend B (F−S interface); (F) blend C (F−S interface).

As shown, as the T_c increases, the degree of cross-linking increases, and the scheme below illustrates cross-linking reactions responsible for the enhanced gel content.

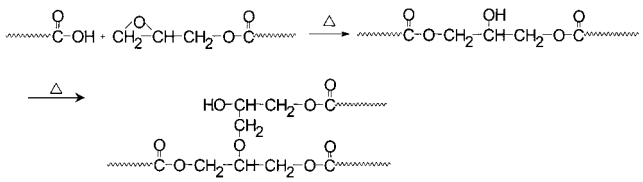

What is also interesting to note is that there are two distinct regions where the gel content changes, and there is a slope change when latexes are coalesced at 90 °C.

Effect of Coalescence Temperature (T_c) on Surfactant Migration. Postponing temporarily the discussion concerned with the gel content, let us compare SDOSS stratification in thermosetting and thermoplastic latex films. For that reason, ATR FT-IR spectra in the 1390−930 cm^{-1} region were recorded from the F−A and F−S interfaces for blends A, B, and C coalesced film at 25 °C. The spectra are shown in Figure 6, traces A and B, C, D, E, and F, respectively. The spectra were recorded approximately from 1.9 μm from the F−A and F−S interfaces, and spectral distortions resulting from refractive index changes were corrected using the

Urban−Huang algorithm.[29] As seen, the SDOSS band at 1046 cm^{-1} is detected at the F−A interfaces for all blends (traces A, B and C) and appears to be stronger in the spectrum recorded from blend A (trace A). However, when the spectra are recorded from the F−S interface, the 1046 cm^{-1} band is not present, indicating that SDOSS migration occurs during film formation for all latex blends. It is somewhat surprising that more SDOSS molecules migrate to the F−A interface in blend A than in blends B and C because blends A and B are thermosetting latexes; thus, one would expect similar behavior at 25 °C. Therefore, further experiments were conducted to investigate this phenomenon.

Previous studies[25] on thermoplastic latexes showed that the temperature difference between T_c and T_g of a latex polymer has a significant effect on coalescence, and thus influence migration of SDOSS. For Sty/*n*-BA copolymer latexes, significantly enhanced SDOSS migration was observed when T_c is above the T_g of the copolymer. On the other hand, for *p*-Sty/*p*-*n*-BA blended latex, SDOSS migration to the F−A interface was observed when $T_c > T_g$ for phase-separated *p*-Sty, which was attributed to increased free volume above the T_g of *p*-Sty phase, thus releasing SDOSS molecules from *p*-Sty particles to the film surface during coalescence. In an effort to determine whether indeed phase separation and the actual T_g of thermosetting films coalesced from blends A and B at 25 °C affect SDOSS behavior, DMTA analysis was performed, and a maximum of tan δ was used as a measure latex film T_g's. The DMTA analysis (not shown) indicated that one maximum attributed to the T_g at 15 °C is present for blend A, and two maxima at 10 and 120 °C for blend B, which are due to T_g's of *p*-nBA/MAA (or p-nBA/GMA) and p-Sty phases, respectively. It should be noted that the T_g's detected for blend B at 10 and 120 °C are slightly higher than the actual T_g for p-nBA/MAA (T_g <0 °C) and p-Sty (T_g = 110 °C), which is most likely due to the presence of slightly cross-linked network in blend B. Similarly to blend B, thermoplastic latex blend C exhibits two T_g at −35 and 110 °C, which are attributed to p-nBA and p-Sty phases, respectively.

With this in mind, let us go back to Figure 6 and realize that when T_c = 25 °C, we detected higher concentration levels of SDOSS near the F−A interface for blend A, which is copolymerized randomly and exhibits single T_g at 15 °C. However, for blends B and C with p-nBA and p-Sty phases, less SDOSS migrates to the F−A interface. These results are consistent with the previous findings for thermoplastic blends of p-Sty/p-nBA latex,[26] which indicated that lower concentration levels of SDOSS migrate to the F−A interface due to the lack of coalescence of the p-Sty phase at T_c = 25 °C.

The effect of T_c on SDOSS migration in thermosetting and thermoplastic latex films can be further examined using ATR FT-IR analysis.[28] Blends A, B, and C were coalesced at 25, 50, 75, 90, 120, and 180 °C for 2 h and cooled to 25 °C, and such films were analyzed using ATR FT-IR to quantitatively determine[28] the SDOSS content changes near the F−A interface as a function of T_c. The 1046 cm^{-1} band due to SDOSS···H_2O interactions was used to quantify the SDOSS···H_2O concentration (linear absorption coefficient is 0.017 L/(mol cm)), and using a double KKT approach,[34] SDOSS volume concentration (C_{vc}) changes as a function of T_c were determined. These results are summarized in Figure 7 and correlate with the gel content of blend A discussed earlier in Figure 5.

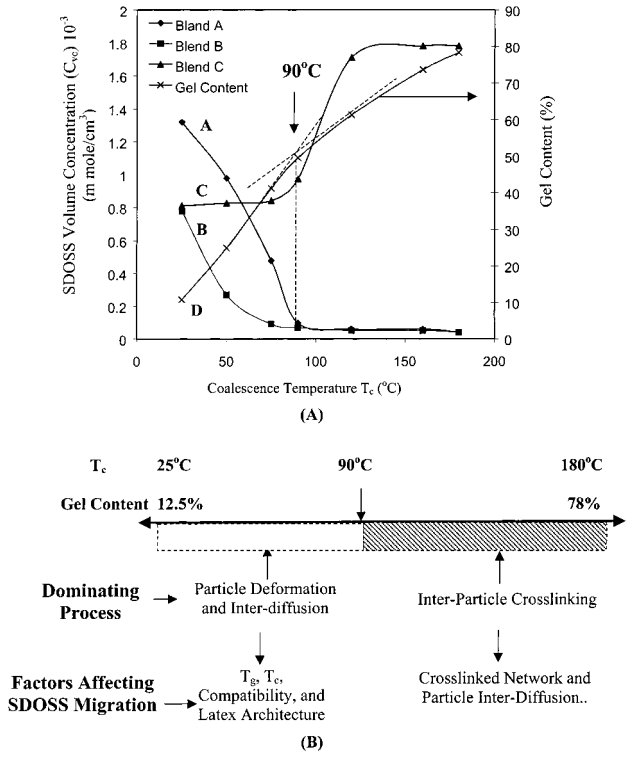

Figure 7. (A) SDOSS volume concentration (V_{vc}) and gel content plotted as a function of T_c for blends A, B, and C. (B) Effect of T_c on dominating processes during latex coalescence.

Because of their thermoplastic compositions, gel contents were not measured for blend C. When T_c = 25 °C, C_{vc} levels are 1.32×10^{-3}, 7.78×10^{-4}, and 7.91×10^{-4} mmol/cm^3 for blends A, B, and C, respectively. For films coalesced from blends A and B, C_{vc} levels decrease with an increase of the T_c, and no SDOSS migration to the F−A interface is detected when T_c > 90 °C. As shown in Figure 7, although SDOSS in blends B and C exhibits similar behavior at 25 °C, when T_c increases, SDOSS migration shows an opposite trend. For blend C, only slight SDOSS increases near the F−A interface is observed when the T_c ranges from 25 to 90 °C. However, when T_c > 90 °C, significant enhancement is observed. These results show that the T_c has different effect on SDOSS migration in thermosetting and thermoplastic latexes. While SDOSS migration is inhibited at higher T_c in thermosetting latex films, significant SDOSS migration to the F−A interface when $T_c > T_g$ of p-Sty in thermoplastic p-Sty/p-nBA latex films is observed. Since during latex coalescence of thermosetting blends A and B containing reactive epoxy groups two processes occur; flow of latex particles and cross-linking reactions, when blends A and B coalesce at elevated temperatures, a highly cross-linked polymer network is formed, and the presence of less permeable network inhibits the mobility of small molecules, such as SDOSS. In fact, this hypnosis is verified by ATR FT-IR results showing that no SDOSS is detected at the F−A interface when T_c > 90 °C in thermosetting blends A and B. In contrast, during thermoplastic blend C coalescence, only flow of latex particles and coalescence occur. In this case, significant enhancement of SDOSS at the F−A interface is observed when $T_c > T_g$ of the p-Sty which is attributed to the increased free volume of the p-Sty phase above its T_g, thus releasing SDOSS from p-Sty particles.

Surfactant Stratification and Latex Coalescence. Previous studies[31] showed that sufficient particle

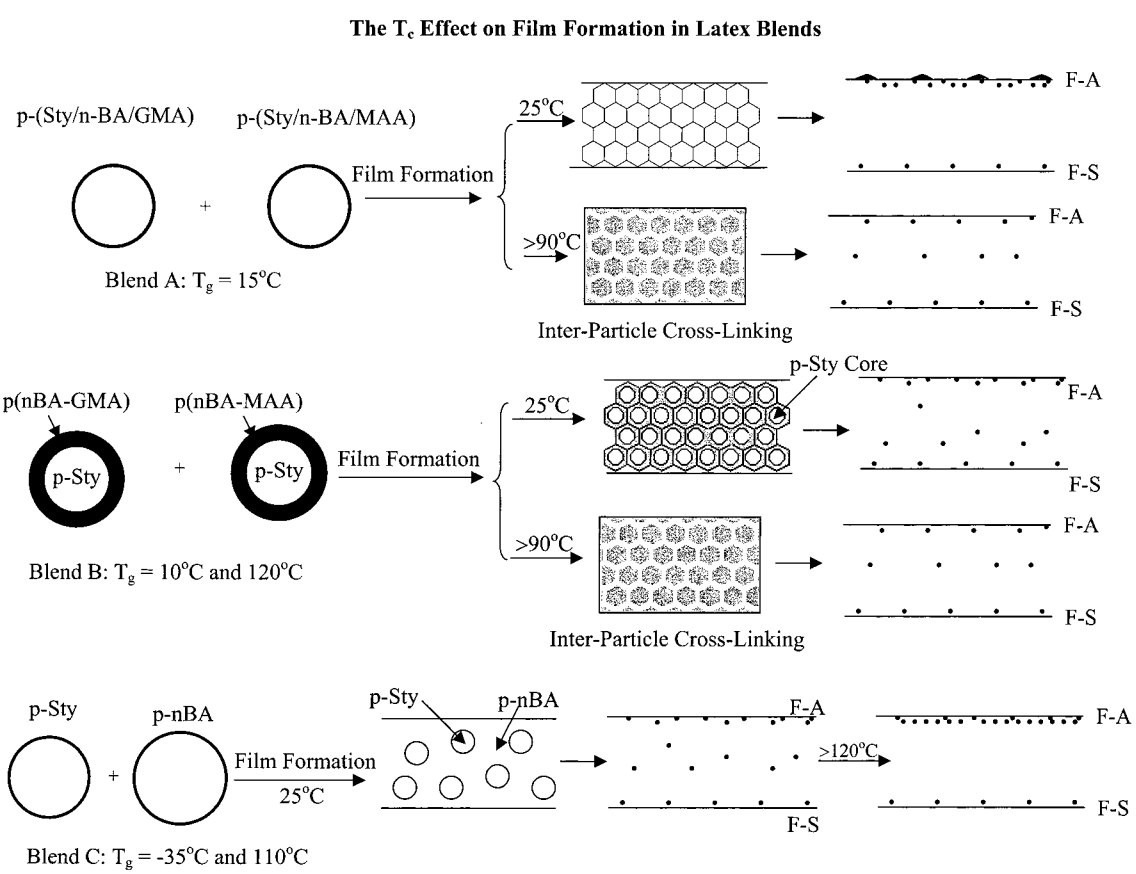

Figure 8. Schematic diagram illustrating the effect of T_c on cross-linking, particle interdiffusion, and SDOSS migration.

deformation and interdiffusion could also cause displacement of surfactants from particle surfaces, which may migrate to the film surface, if compatibility between surfactant and polymer is poor. This process can potentially compete with a water flux, but in thermosetting latex films, dynamics of cross-linking and particle interdiffusion is controlled by the T_c, and the particle interdiffusion is favorable at lower T_c, as oppose to cross-linking, which is enhanced at higher T_c. It should be noted that there are interparticle cross-linking reactions in blends A and B at elevated temperature because reactive sites are present on particle surfaces. As seen in Figure 7A, the effect of the T_c on the SDOSS migration is amplified, indicating that cross-linking and interdiffusion play a key role on SDOSS behavior. In this case, migration of SDOSS to the F−A interface at low T_c is attributed to sufficient particle interdiffusion and poor compatibility between SDOSS/polymer during water flux. On the other hand, at elevated temperatures, if kinetics of interparticle cross-linking is faster than interdiffusion across particle surface boundaries, latex particles may exhibit limited coalescence. As a result, SDOSS migration will be completely inhibited due to highly cross-linked network and limited particle interdiffusion. In fact, SDOSS migration is completely inhibited when T_c > 90 °C for blends A and B. Therefore, ATR FT-IR quantitative analysis (Figure 7A) and swelling experiments (Figure 5) show that there is a significant effect of the T_c on competing cross-linking, particle interdiffusion, and SDOSS migration, and these processes are inherently related. Figure 7B depicts what factors affect SDOSS migration as well as dominating processes as a function of T_c.

Based on these results, a schematic diagram shown in Figure 8 illustrating blends A, B, and C latex film formation was constructed. For blend A, when particle−particle interdiffusion is a predominating process at 25 °C, SDOSS migration occurs due to poor compatibility between SDOSS/polymer. For blend B, less SDOSS molecules migrate to the F−A interface due to lack of coalescence of the p-Sty phase,[25] which is demonstrated by two T_g's at 10 and 120 °C due to p-nBA/MAA and p-Sty phases, respectively. However, at elevated temperatures, when cross-linking is a dominating process, SDOSS molecules are entrapped due to increased cross-linking and limited particle interdiffusion. For thermoplastic blend C containing hard p-Sty and soft p-nBA particles, SDOSS molecules migrate to the F−A interface when T_c > T_g of the p-Sty phase as a result of the increased free volume of the p-Sty phase.

Transient Effects during Coalescence. Although we addressed the issue of mobility and stratification of individual components in latexes in a number of previous studies,[20−25] their relevance becomes even more pronounced in the context of latex films examined in this paper. In essence, the real question is, can surfactants be seen at various coalescence stages, and if so, how are surface interfacial properties affected? In an effort to examine SDOSS behavior at various stages of the film formation, microscopic ATR FT-IR was performed. In Figure 9A, a, b, c, and d illustrate images obtained from the F−A interface of blend A recorded after 0, 15, 27, and 33 h of coalescence at 25 °C. As seen, the surface becomes rougher when going from image a to d, showing formation of aggregates, which are very pronounced after coalescence times exceed 27 h. In an effort to correlate surface compositional changes with coalescence times, ATR FT-IR microanalysis was performed, which was accomplished by recording the spectra using an ATR crystal on the surface area of 50−

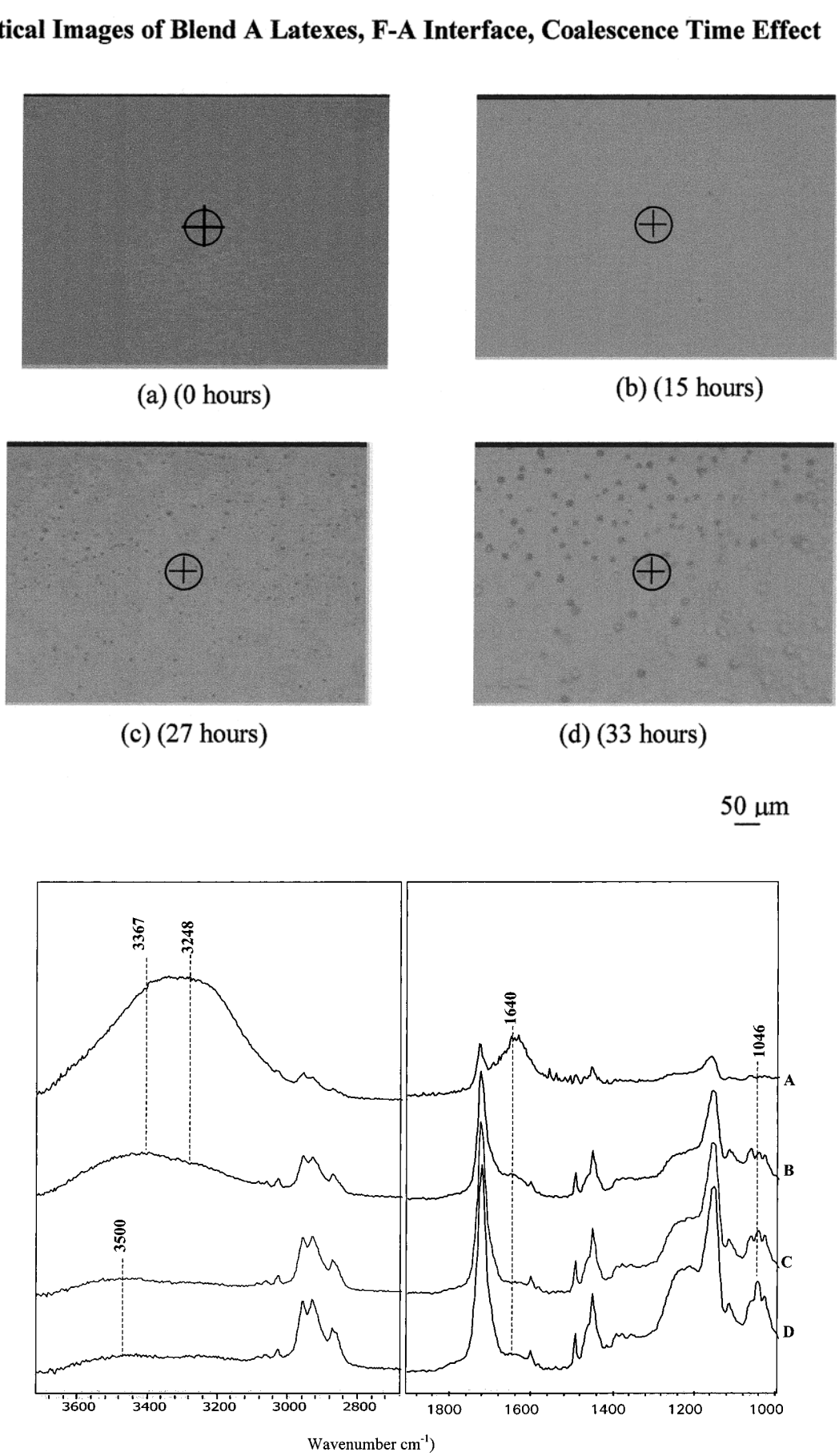

Figure 9. (A, upper) FT-IR images of films obtained from blend A; the F−A interface; coalescence times: (a) 0 h; (b) 15 h; (c) 27 h; (d) 33 h. (B, lower) Microscopic ATR FT-IR spectra of blend A recorded from the F−A interface at different coalescence times: (A) 0 h; (B) 15 h; (C) 27 h; (D) 33 h.

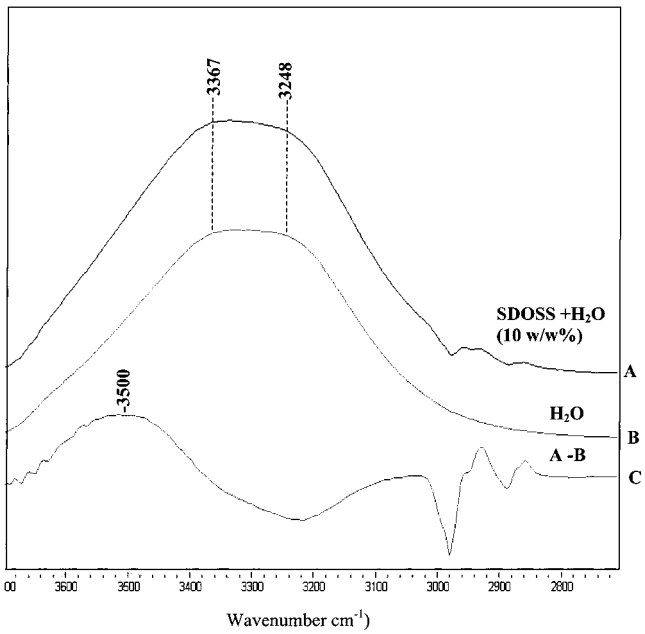

Figure 10. Transmission FT-IR spectra in the OH stretching region of H_2O: (A) SDOSS + H_2O (10 w/w %); (B) H_2O (DDI); (C) difference spectrum A − B.

100 μm. A marker "+" at the center of each image of Figure 9A, a, b, c, and d indicates spectral acquisition areas, and the resulting spectra are presented in Figure 9B, traces A, B, C, and D. These series of spectra were recorded from the F−A interface show that the bands at 3367, 3248, and 1640 cm^{-1} due to OH stretching and bending modes of H_2O decrease as coalescence progresses and are no longer detected after 27 h. Instead, a new broad band at 3500 cm^{-1} is present. During coalescence the 1046 cm^{-1} band due to SDOSS is detected when coalescence times approach 15 h, and its intensity becomes more pronounced at extended coalescence times. Thus, aggregates observed in Figure 9A are mainly composed of SDOSS domains, and their concentration levels increase significantly as coalescence processes.

Another intriguing features in these data are the changes in water bands in the 3500−3200 cm^{-1} region. As shown in Figure 9B, water bands at 3367 and 3248 cm^{-1} decrease to minimum when H_2O is removed from the film. At the same time, SDOSS becomes more pronounced near the F−A interface, and the new band at 3500 cm^{-1} is observed. Although one would perhaps pay a little attention to these observations, our previous experience showed that the OH stretching region may provide quite useful information. For this reason, we collect transmission spectra of SDOSS dissolved in H_2O (10 w/w %), pure H_2O (DDI), and subtracted pure H_2O contribution from the spectrum of SDOSS/H_2O mixture. The results are shown in Figure 10, traces A, B, and C, respectively. It is quite apparent that the subtraction of the H_2O spectrum results in the presence of the 3500 cm^{-1} band, which is due to interactions between H_2O and SDOSS molecules. Thus, there are three bands in the OH stretching region, which is not surprising because water itself exhibits two bands in this region due to free and H-bonded OH vibrations,[32] and the 3500 cm^{-1} band results from $SO_3^-Na^+-H_2O$ interactions. Similar observations were made for OH stretching bands in salt or acid/salt aqueous environments.[33]

At this point it is appropriate to correlate transient concentration changes of SDOSS with coalescence times

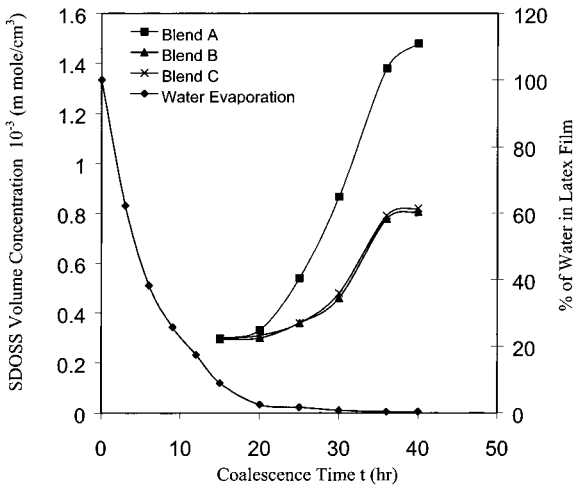

Figure 11. SDOSS volume concentration changes and percent of water retention in latex films plotted as a function of coalescence time.

for blends A, B, and C. This can be accomplished by quantifying spectroscopic information at various coalescence intervals. These results are summarized in Figure 11 for T_c = 25 °C, where the amount of SDOSS migration to the F−A interface and relative amounts of H_2O left in the latex films are plotted as a function of coalescence times. A percent fraction of H_2O left in the film was calculated using the 3367 cm^{-1} band intensity ratio I_t/I_0, where I_t and I_0 are the 3367 cm^{-1} band intensities at a given time t ratioed to initial I_0 intensity at t = 0 h. It should be noted that the amount of water detected using ATR is assumed to be similar across the film thickness, which is reasonable since in order for water to be removed from the film, migration to the surface is required. As shown in Figure 12, about 95% of H_2O evaporates from latex films when coalescence times approach 20 h. At the same time, only small fraction of SDOSS migrates to the F−A interface. However, as soon as the water content is less than 5%, SDOSS molecules begin to diffuse to the F−A interface, and their concentration levels increase significantly over the next 16 h of coalescence, after which time they level off. Analysis of the data presented in Figure 11 also illustrates that there is a distinct difference between the behavior of blends A and B, which exhibit the same trends, and blend C. As is shown in Figure 7, after 36 h of coalescence at 25 °C, SDOSS V_{vc} are 1.32×10^{-3}, 7.78×10^{-4}, and 7.91×10^{-4} mmol/cm^3 for films obtained from blends A, B, and C, respectively. Since blend A exhibits one T_g, which is 10 °C belong the T_c, and virtually no cross-linking occurs during coalescence, surfactant molecules are capable of migrating faster to the F−A interface.

Conclusions

There are a number of points that these studies allow us to make: (1) Although one would expect that SDOSS will migrate to the F−A interface with water flux, this is not the case. As a matter of fact, SDOSS migrates to the surface after water is almost entirely removed from the film. (2) Processes occurring during film formation are inherently affecting surfactant migration, and cross-linking along the particle−particle interdiffusion play an important role. (3) An extent of the surfactant migration can be altered by surface particle morphology as well as cross-linking reactions. (4) In contrast to other

imaging tools like AFM, IR and Raman spectroscopies are capable of obtaining quite powerful molecular level information from latex films.

Acknowledgment. The authors are thankful to the National Science Foundation Industry/University Cooperative Research Center in Coatings (Grant EEC 0002775) at the University of Southern Mississippi and Eastern Michigan University for support of these studies.

References and Notes

(1) Odeberg, J.; Rassing, J.; Jonsson, J.; Wesslen, B. *J. Appl. Polym. Sci.* **1998**, *70*, 897.
(2) Chu, F.; Mckenna, T. F. *Polymer* **1997**, *38*, 6157.
(3) Zosel, A.; Ley, G. *Macromolecules* **1993**, *26*, 2222.
(4) Mohammed, E. S.; Daniels, L. H.; Sperling, A. K.; El-Aasser, M. S. *J. Appl. Polym. Sci.* **1997**, *66*, 1869.
(5) Winnik, M. A.; Pinenq, P.; Kruger, C.; Zhang, Jianxin *J. Coat. Technol.* **1999**, *71*, 892, 47.
(6) Niu, B.-J.; Urban, M. W. *J. Appl. Polym. Sci.* **1995**, *56*, 377.
(7) Niu, B.-J.; Urban, M. W. *J. Appl. Polym. Sci.* **1996**, *60*, 371.
(8) Urban, M. W.; Evanson, K. W. *Polym. Commun.* **1990**, *31*, 279.
(9) Thorstenson, T. A.; Evanson, K. W.; Urban, M. W. *Polym. Mater. Sci. Eng.* **1991**, *64*, 195.
(10) Thorstenson, T. A.; Tebelius, L. K.; Urban, M. W. *J. Appl. Polym. Sci.* **1993**, *49*, 103.
(11) Evanson, K. W.; Thorstenson, T. A.; Urban, M. W. *J. Appl. Polym. Sci.* **1991**, *42*, 2309.
(12) Thorstenson, T. A.; Evanson, K. W.; Urban, M. W. In *Advances in Chemistry Series Vol. 236*; Urban, M. W., Craver, C. D., Eds.; American Chemical Society: Washington, DC, 1993.
(13) Evanson, K. W.; Urban, M. W. In *Surface Phenomena and Fine Particles in Water-Based Coating and Printing Technology*; Sharma, M. K., Micale, F. J., Eds.; Plenum: New York, 1991; p 197.
(14) Thorstenson, T. A.; Urban, M. W. *J. Appl. Polym. Sci.* **1993**, *47*, 1387.
(15) Thorstenson, T. A.; Urban, M. W. *J. Appl. Polym. Sci.* **1993**, *50*, 1207.
(16) Niu, B.-J.; Urban, M. W. *J. Appl. Polym. Sci.* **1996**, *60*, 389.
(17) Evanson, K. W.; Thorstenson, T. A.; Urban, M. W. *J. Appl. Polym. Sci.* **1991**, *42*, 2297.
(18) Evanson, K. W.; Urban, M. W. *J. Appl. Polym. Sci.* **1991,** *42*, 2287.
(19) Kunkel, J. P. W.; Urban, M. W. *J. Appl. Polym. Sci.* **1993**, *50*, 1217.
(20) Tebelius, L. K.; Urban, M. W. *J. Appl. Polym. Sci.* **1995**, *56*, 387.
(21) Zhao, C. L.; Holl, Y.; Pith, T.; Lambla, M. *Colloid Polym. Sci.* **1987**, *265*, 823.
(22) Zhao, Y.; Urban, M. W. *ACS Polym. Mater. Eng.* **1998**, *78*, 25.
(23) Thorstenson, T. A.; Urban, M. W. *J. Appl. Polym. Sci.* **1993**, *47*, 1381.
(24) Niu, B.-J.; Urban, M. W. *J. Appl. Polym. Sci.* **1996**, *60*, 379.
(25) Zhao, Y.; Urban, M. W. *Macromolecules*, in press.
(26) Zhao, Y.; Urban, M. W. *Macromolecules*, in press.
(27) Dollish, F. R.; Fateley, W. G.; Bentley, F. F. *Characteristic Raman Frequencies of Organic Compounds*; Wiley-Interscience: New York, 1973; p 191.
(28) Vitali, R.; Montani, E. *Polymer* **1980**, *21*, 1220.
(29) Urban, M. W. *Attenuated Total Reflectance Spectroscopy of Polymers; Theory and Practice*; American Chemical Society: Washington, DC, 1996.
(30) Pepper, K. W.; Reichenberg, D.; Hale, D. K. *J. Chem. Soc.* **1952**, *4*, 3129.
(31) Chevalier, Y.; Pichot, C.; Graillat, C.; Joanicot, M.; Wong, K.; Maquet, J.; Lindner, P.; Cabane, B. *Colloid Polym. Sci.* **1992**, *270*, 806.
(32) Reimers, J. R.; Watts, R. O. *Chem. Phys.* **1984**, *91*, 201.
(33) Urban, M. W.; Koenig, J. L. *Appl. Spectrosc.* **1987**, *41*, 590.
(34) The average depth thickness was determined in the following equation: $d_p = \lambda_0/[2\pi\eta_1(\sin^2\theta - \eta_{21})^{1/2}]$, where λ_0 is wavelength of light, η_1 is refractive index of crystal, θ is angle of incidence, and η_{21} is the refractive index ratio of sample and crystal. All spectra were corrected using the Urban−Huang algorithm[29] to remove spectral distortions resulting from refractive index changes.

MA000625H